Eur. Phys. J. B **45**, 339–345 (2005)
DOI: 10.1140/epjb/e2005-00191-6

THE EUROPEAN PHYSICAL JOURNAL B

Multi-mode transport through a quantum nanowire with two embedded dots

Vidar Gudmundsson[1,a], Gudny Gudmundsdottir[1], Jens Hjorleifur Bardarson[1], Ingibjorg Magnusdottir[1], Chi-Shung Tang[2], and Andrei Manolescu[1]

[1] Science Institute, University of Iceland, Dunhaga 3, 107 Reykjavik, Iceland
[2] Physics Division, National Center for Theoretical Sciences, P.O. Box 2-131, Hsinchu 30013, Taiwan

Received 1st December 2004 / Received in final form 8 March 2005
Published online 6 July 2005 –

Abstract. We investigate the conductance of a quantum wire with two embedded quantum dots using a T-matrix approach based on the Lippmann-Schwinger formalism. The quantum dots are represented by a quantum well with Gaussian shape and the wire is two-dimensional with parabolic confinement in the transverse direction. In a broad wire the transport can assume a strong nonadiabatic character and the conductance manifests effects caused by intertwined inter- and intra-dot processes that are identified by analysis of the "nearfield" probability distribution of the transported electrons.

PACS. 73.63.Nm Quantum wires – 73.23.Ad Ballistic transport – 75.47.Jn Ballistic magnetoresistance

1 Introduction

Transport through vertical or lateral double dot systems has been investigated by many groups experimentally [1–6] or theoretically [7–13], just to mention few. In most of these models the researchers use effective Hubbard-type models or exact diagonalization for few electrons in order to describe the effects of higher order correlations on the electron transport. Other studies have focused on describing the effects of the interaction of the geometry of the leads and the quantum dot, where commonly, the system tracted is a dot embedded in a quantum wire [14,15]. The focus has then been on resonances caused by the interplay of the discrete quasi-bound states of the dot and the continuum of the wire [16,17], or earlier on quantum bound states in a classically unbound system of crossed wires [18].

To describe the transport process various implementations of a transfer-matrix method have been used [14, 15,19–21], nonequilibrium Greens functions [22], or methods built on the Lippmann-Schwinger approach to scattering [23–26]. Not forgetting that similar methods have been applied in the rich field of molecular transport where commonly nonequilibrium Greens functions [27] or a Lippmann-Schwinger approach [28] have been used in combination with a DFT formalism.

In a broad wire the scattering center or centers can lead to a complex mixing of subbands that has often been analyzed in numerical calculations by monitoring the intersubband transmission coefficients. Here we apply an approach built on the Lippmann-Schwinger formalism that can handle a wide range of smooth scattering potentials embedded in a quantum wire, and which allows us to access the probability distribution of the electrons in the wire [23,25].

It is well known that transmission of electrons through a quantum dot shows resonance structures. For the case of a weakly coupled dot – dot in which electrons are separated from the connecting leads by tunneling barriers – the resonance peaks in the transmission are due to the alignment of the incident electron energy with the quasi-bound levels in the dot [29–31]. Interestingly, the quasi-bound levels of similar nature still exist in the case of an open quantum dot – where tunneling barriers between the dot and the lead are absent. These quasi-bound levels are strongly coupled to the wire, and give also rise to resonances in the transmission. However, resonantly reflected dip structures, rather than resonantly transmitted peaks structures, become the signatures for the resonances.

We investigate a system composed of a quasi two-dimensional quantum wire in no external magnetic field with a parabolic confinement in the direction transverse to the transport. Embedded laterally in the quantum wire we have two identical quantum dots with their centers separated by the distance $2d$, but the effective size of the smoothly Gaussian shaped dots is on the order of $d/8$. We shall consider a narrow wire chosen such that the depth of the dot is a bit larger than the energy separation of the unperturbed subbands of the wire, and a broad wire where the subband separation is only 1/10 of the dot depth. We

[a] e-mail: vidar@raunvis.hi.is

consider two different dot sizes, but in both cases the effective size of the dot does not broaden the wire. We are thus considering a wire with embedded dots in between the limit where the dots are similar to an impurity represented by attractive δ-functions, and the case where the dots can be considered of the same width or wider than the wire. We assume the electrons to be incident in some of the lowest lying energy subbands of the wire, but due to the geometry of the system we have to include several more subbands in the calculation in order to describe the transport correctly.

Here the dots are far enough apart that correlation effects should be minimal, but the mode mixing and the interplay of the inter- and intra dot processes should be large. The probability density of the electrons will turn out to give us an excellent insight into what is happening in the system when the conduction is far more complex than in an ideal wire.

The experimental systems most likely to be able to fulfill our conditions on model parameters are quantum wire and dots systems electrostatically defined in semiconductor heterostructures with gates and/or backgates.

2 Models

We consider a multi-mode transport of electrons along the z-direction through a two-dimensional quantum wire defined by a parabolic confinement in the x-direction with the characteristic frequency $E_0 = \hbar\Omega_0$. The electrons incident from the left ($z \to -\infty$) impinge on a scattering potential composed of two Gaussian wells located at $z = \pm d$

$$V_{sc} = V_0 \left\{ e^{-\beta((z-d)^2+x^2)} + e^{-\beta((z+d)^2+x^2)} \right\}. \quad (1)$$

The scattering modes are expanded in the transverse modes χ_m

$$\psi^+_{nE}(\mathbf{r}) = \sum_m \varphi^n_{mE}(z)\chi_m(x), \quad (2)$$

that are the eigenmodes of the parabolic confinement of the quantum wire. An incident electron with energy $E = \hbar^2 k_n^2(E)/(2m) + \epsilon_n$, where $\epsilon_n = \hbar\Omega_0(n + 1/2)$ can propagate in mode n if $\epsilon_n < E$ otherwise the state is evanescent. We use the coupled multi-mode Lippmann-Schwinger equations [32,33] to establish a set of coupled integral equations for the T-matrix [23] which in turn is used to calculate the transmission amplitude that within the Landauer formalism leads to the linear response conductance at vanishing temperature [34,35]

$$G = \frac{2e^2}{h}\mathrm{Tr}[t^\dagger t]. \quad (3)$$

The T-matrix can also be used to construct the probability density of the scattering states through their wave functions [23]

$$\phi^n_{mE}(z) = \phi^{n0}_{mE}(z) + \frac{m}{\pi\hbar^2}\int_{-\infty}^{+\infty} dp \frac{\sqrt{|p|}e^{ipz}}{k_m^2 - p^2} T_{mn}(p, k_n). \quad (4)$$

All matrix elements have been calculated analytically and special care has been taken to include enough modes in the numerical calculations to reach convergent solutions. The singular part of the integration for the scattering states (4) and the T-matrix has been completed analytically [23].

The mirror symmetry of the scattering potential (1) along the center, $x = 0$, of the wire results in finite matrix elements only between transverse modes of the same parity.

3 Results

We shall consider a broad ($E_0 = \hbar\Omega_0 = 1$ meV) or a narrow ($E_0 = \hbar\Omega_0 = 6$ meV) quantum wire with two identical embedded quantum dots located at $z = \pm d$. The dots are small, with $\beta = 0.01$ nm^{-2}, or larger with $\beta = 0.003$ nm^{-2} in equation (1). The depth of the dots or wells is $V_0 = -10$ meV, and we assume GaAs parameters yielding the effective Bohr radius $a_0 = 9.79$ nm, and the Rydberg $Ry = 5.92$ meV. Clearly, we can expect the transport to vary strongly with the width of the wire since in the case of the broad wire in Figure 1 several subbands or modes can be coupled by the scattering potential. In the narrow wire the characteristic length $a_w = \sqrt{\hbar/(m\Omega_0)} = 13.8$ nm, in the broad one $a_w = 33.7$ nm.

3.1 Narrow wire

The conductance of the narrow wire is shown in Figure 2 for both types of dots as function of the parameter $X = E/E_0 + 1/2$, whose integral part numbers the propagating subbands participating in the transport at a particular energy E. The figure indicates that the main role of the dots in the narrow wire is to define a semitransparent cavity in between them. In the case of the small dots this cavity has a well defined length and well known geometrical resonances are seen in the conductance as the separation, d, of the dots is increased. When the dots are larger (lower panel) the higher order resonances vanish and one or two dips occur in the conductance, characteristic of an attractive scattering potential. For the smallest separation of the dots, when they partially overlap we see two dips. In Figure 3 we present the probability density for three relevant cases in order to better understand the microscopic processes in the system. In Figure 3a we see the probability density for the large dots corresponding to the lowest resonance in the lower panel of Figure 2, when $d = 8a_0$. As expected the main probability density is located in the cavity between the dots. Interestingly, due to the finite size of the dots we also see a small density at the location of each dot. Here the electrons enter the system in the lowest mode $n = 0$ and exit the system in the same mode, this together with the total transmission leads to a constant probability density in the wire away from the scattering potential. In Figures 3b and c we see the probability density at the dips for the large dots as $d = 2a_0$. The two states causing the dips are the symmetric and

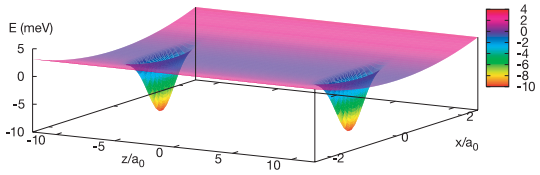

Fig. 1. (Color online) The broad quantum wire with two embedded large dots. The two horizontal axes are not drawn in the same scale, the dot potentials (4) are circular. $E_0 = \hbar\Omega_0 = 1.0$ meV, $V_0 = -10$ meV, $\beta a_w^2 = 0.571$, $a_w = 33.7$ nm, and for GaAs $a_0 = 9.79$ nm.

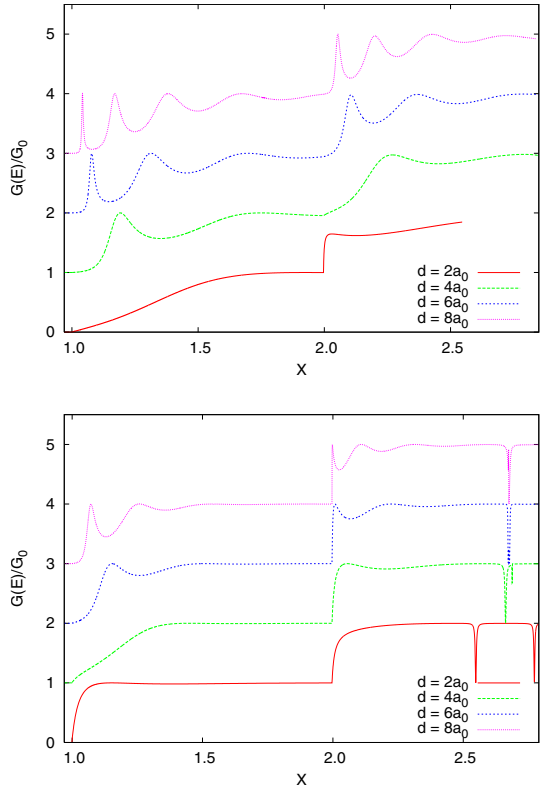

Fig. 2. (Color online) The conductance in units of $G_0 = 2e^2/h$ of a narrow parabolic wire with embedded small dots $\beta a_w^2 = 1.90$ (upper panel), and large dots $\beta a_w^2 = 0.571$ (lower panel) for different displacement $z = \pm d$ from the center of the wire $z = 0$ as function of $X = E/E_0 + 1/2$. $E_0 = \hbar\Omega_0 = 6.0$ meV, $V_0 = -10$ meV, $a_w = 13.8$ nm, and for GaAs $a_0 = 9.79$ nm.

the anti-symmetric quasi-bound state, the latter one occurring at a bit higher energy as expected. The structure of the density in either case reminds us that due to the high symmetry of the dot potential, equation (1), the evanescent state causing the reflection of the $n = 0$ mode is in the third subband with $n = 2$ and is thus broader than the resonant state in Figure 3a. Due to the high probability density of the electrons in the evanescent state we do barely see the incoming and the reflected density on the left side of the scattering potential on the chosen color scale.

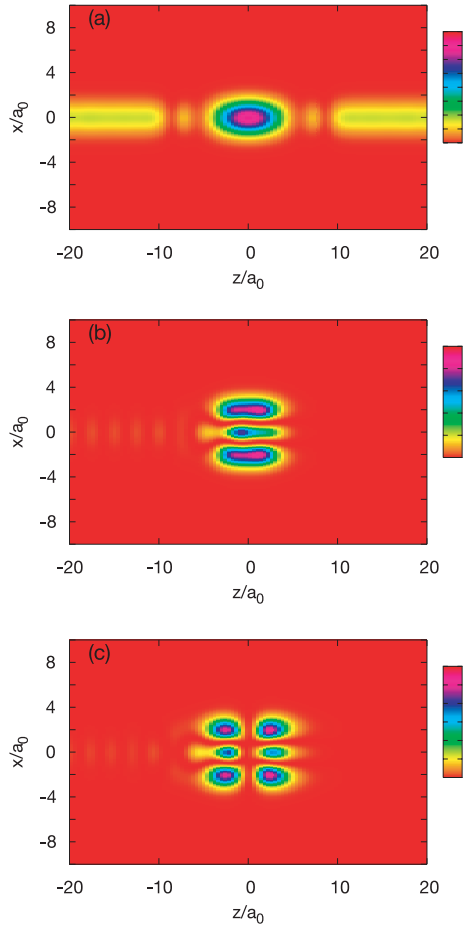

Fig. 3. (Color online) The probability density of the scattering state $\psi_E(x, y)$ in the narrow quantum wire in the presence of two embedded large dots. The incident energy of the $n = 0$ mode corresponds to $X = 1.08$ and $d = 8a_0$ (a), $X = 2.58$ and $d = 2a_0$ (b), and $X = 2.80$ and $d = 2a_0$ (c), corresponding to the peak and the two dips, respectively, in the conductance in the lower panel of Figure 2. $E_0 = \hbar\Omega_0 = 6.0$ meV, $V_0 = -10$ meV, $a_w = 13.8$ nm, $\beta a_w^2 = 0.571$.

3.2 Broad wire

In order to prepare the analyses of the conduction of a broad quantum wire ($E_0 = 1$ meV) with two embedded dots we first show in the upper panel of Figure 4 the conduction in the broad wire with only one quantum dot embedded, large or small. The sharp dip seen at the end of the second conduction step in a narrow wire is turned into a broad minimum in the broad wire due to the stronger coupling between the subbands caused by the dot in the broad wire.

In the lower panel of Figure 4 we display the conductance of the broad wire with the two embedded dots at $d = 8a_0$. The presence of the two well separated dots adds considerably to the fine structure of the conductance compared to the results for one dot. Moreover, this structure involves the coupling of many subbands and thus requires the inclusion of approximately 16 of them in the numerical calculation in order to reach well converged results.

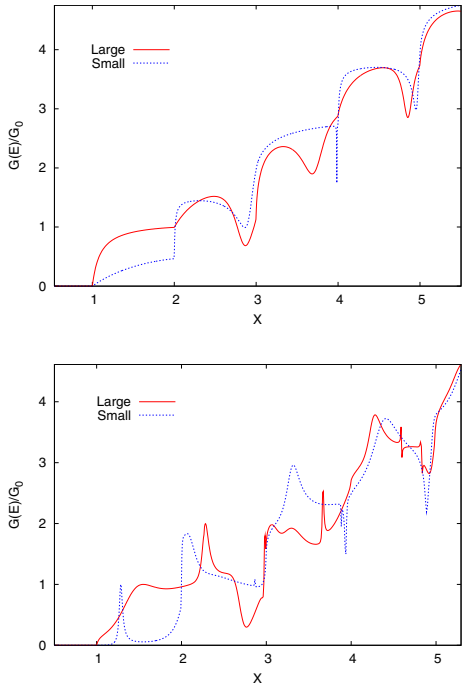

Fig. 4. (Color online) The conductance in units of $G_0 = 2e^2/h$ of a broad wire with one embedded dot at the center $z = 0$, (upper panel), and two dots at $z = \pm 8a_0$, (lower panel) as function of $X = E/E_0 + 1/2$. $E_0 = \hbar\Omega_0 = 1.0$ meV, $V_0 = -10$ meV, $a_w = 33.7$ nm, and for GaAs $a_0 = 9.79$ nm. A small dot is characterized by $\beta a_w^2 = 11.37$ and a large one by $\beta a_w^2 = 3.41$.

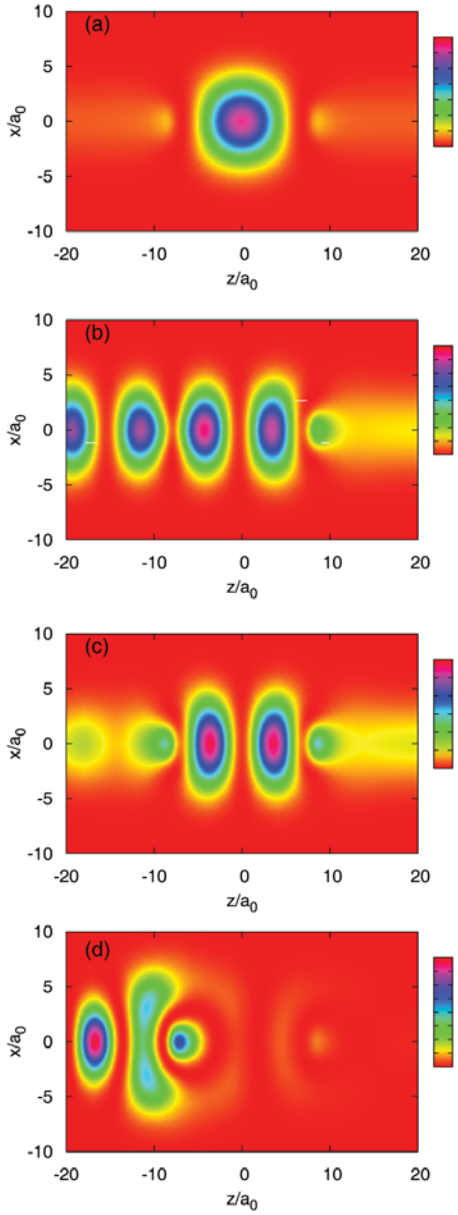

Fig. 5. (Color online) The probability density of the scattering state $\psi_E(x, y)$ in the broad quantum wire in the presence of two small embedded dots centered at $z = \pm 8a_0$. The incident energy and modes correspond to: (a) $X = 1.284$ and $n = 0$, (b) $X = 1.98$ and $n = 0$, (c) $X = 2.07$ and $n = 0$, and (d) $X = 2.76$ and $n = 0$. $E_0 = \hbar\Omega_0 = 1.0$ meV, $V_0 = -10$ meV, $a_w = 33.7$ nm, and $\beta a_w^2 = 11.37$.

First, we start with the electron probability density shown in Figure 5 to gain insight into the multitude of processes taking place in the case of the small dots. Similarly, as in the case of the narrow wire we have a transmission resonance at $X = 1.284$ caused by a state located in the "cavity" between the dots shown in Figure 5a. We also see small probability maxima at the dots themselves. The second transmission resonance at $X = 2.07$ is caused by the next mode in the inter-dot cavity and is shown in Figure 5c, but it is also interesting to check the probability density at a bit lower energy $X = 1.98$, see Figure 5b. Here there is considerable reflection and as the figure shows this can be interpreted as the electrons being reflected by the second dot, the first dot simply loses its effects in a minimum in the interference between the incoming and reflected wave. Thus, by increasing the energy to $X = 2.76$ we observe a reflection by the first dot in Figure 5d. The valley structure in G around $X = 2.76$ corresponds to the electrons making inter-subband transitions from $n = 0$ to the subband threshold of the third subband ($n = 2$) forming a quasi-bound state. The wide valley structure implies a short life time of such a state.

At $X = 2.86$ we see a narrow resonance in the conduction. The corresponding probability density in Figure 6 has the typical structure of an evanescent state in the third subband for the incoming $n = 0$ state and a normal conducting mode for the $n = 1$ instate. The evanescent state clearly belongs mainly to the first dot, but is also fairly extended into the inter-dot cavity.

To finish the observation of the case of the small dots we examine the electronic probability density for the two narrow dips found at $X = 3.88$, and 3.94. These are presented in Figure 7 for the two lowest incoming modes $n = 0$ and 1. Here the first and the third mode conduct partially, as can be confirmed for the $n = 0$ mode in Figures 7a and c. The two $n = 0$ modes are almost identical, but the second incoming mode $n = 1$ is reflected due to an

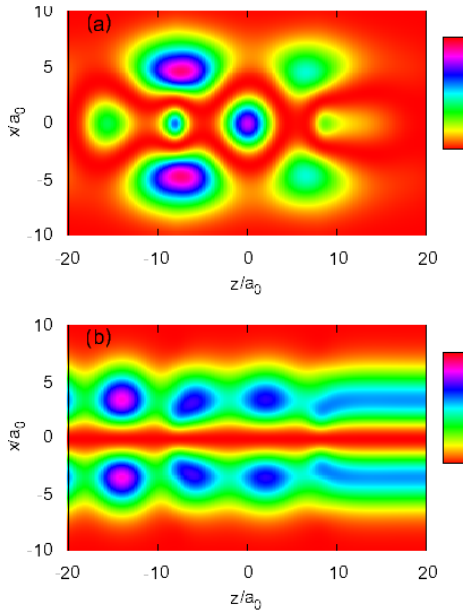

Fig. 6. (Color online) The probability density of the scattering state $\psi_E(x, y)$ in the broad quantum wire in the presence of two small embedded dots centered at $z = \pm 8a_0$. The incident energy and modes correspond to: (a) $X = 2.86$ and $n = 0$, (b) $X = 2.86$ and $n = 1$. $E_0 = \hbar\Omega_0 = 1.0$ meV, $V_0 = -10$ meV, $a_w = 33.7$ nm, and $\beta a_w^2 = 11.37$.

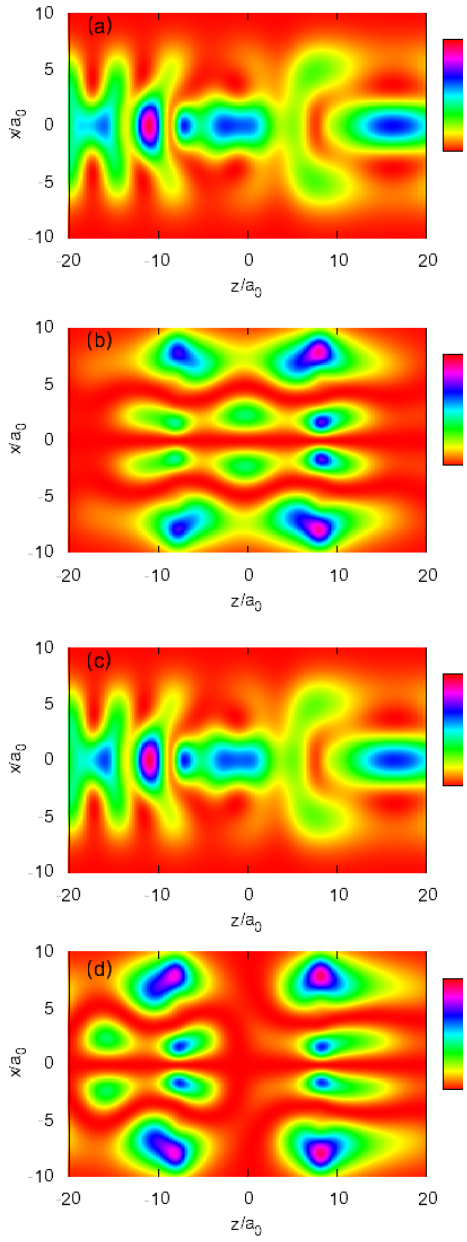

Fig. 7. (Color online) The probability density of the scattering state $\psi_E(x, y)$ in the broad quantum wire in the presence of two small embedded dots centered at $z = \pm 8a_0$. The incident energy and modes correspond to: (a) $X = 3.88$ and $n = 0$, (b) $X = 3.88$ and $n = 1$, (c) $X = 3.94$ and $n = 0$, and (d) $X = 3.94$ and $n = 1$. $E_0 = \hbar\Omega_0 = 1.0$ meV, $V_0 = -10$ meV, $a_w = 33.7$ nm, and $\beta a_w^2 = 11.37$.

interaction with an evanescent mode in the fourth $n = 3$ subband. The evanescent modes in Figures 7b and d show the symmetry of the fourth band and are the distinct two lowest symmetric and antisymmetric quasi-bound states of the dot system.

The system with larger dots allows for a richer mixture of intra and inter-dot processes or states. The lowest transmission resonance is now a broad feature with a corresponding electronic probability density that is a clear superposition of a state in the inter-dot cavity and states located at each dot, see Figure 8a. The next transmission resonance at $X = 2.28$ is narrow and for the incoming $n = 0$ mode is composed of a state with a high proportion of a p_z-type atomic orbital or higher on each dot as the probability in Figure 8b shows. The $n = 1$ in-mode on the other hand is basically a p_y-type state in the inter-dot cavity and to lesser degree p_y-states at each dot, see Figure 8c. In the conductance minimum at $X = 2.77$ we observe the familiar evanescent mode (Fig. 8d) in the third subband reflecting a large portion of the incoming wave.

At $X = 3.67$ the conductance displays a narrow resonance that is caused by an evanescent state in the fourth subband interacting with the second incoming mode as can be verified by the probability density shown in Figure 9b. Here is also curious to note that the scattering potential mixes up the first and the third incoming modes; Figure 9a shows the incoming $n = 0$ state leaving the scattering region in the $n = 2$ mode, and the opposite process is seen happening in Figure 9c. In the first case there is a considerable probability for the electron in the first dot, and in the second case this is reversed. Here, one should remember that even though we talk about large dots in this case the effective size of the dots is comparable to the width of the incoming state and thus the third mode is quite broader than the dot, and the broadness of the wire leads to large matrix elements between the the first and the third mode of the wire. This mixing of incoming states, a character of nonadiabatic transport, or crosstalk between the channels or modes, is not limited to the peak

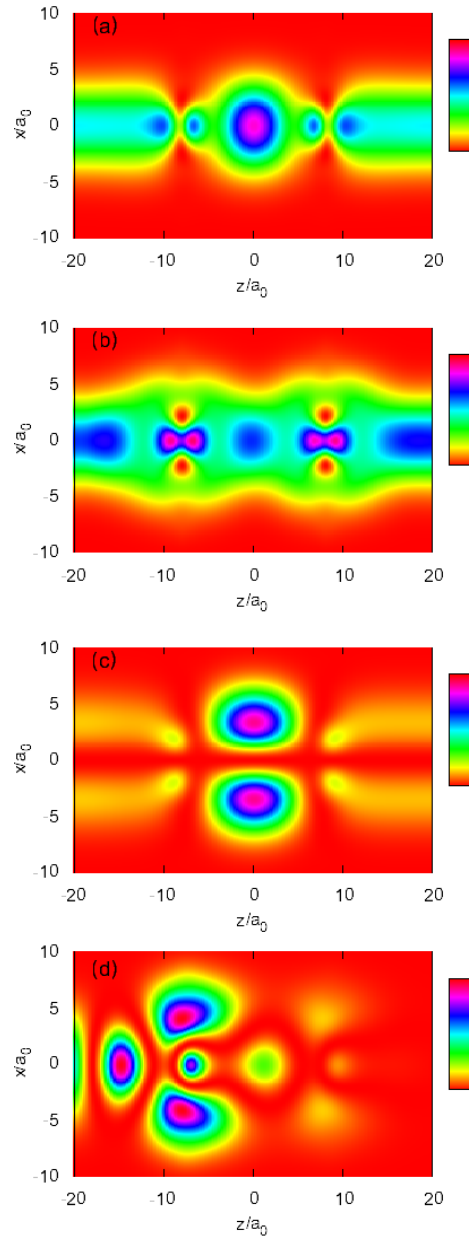

Fig. 8. (Color online) The probability density of the scattering state $\psi_E(x, y)$ in the broad quantum wire in the presence of two large embedded dots centered at $z = \pm 8a_0$. The incident energy and modes correspond to: (a) $X = 1.55$ and $n = 0$, (b) $X = 2.28$ and $n = 0$, (c) $X = 2.28$ and $n = 1$, (d) $X = 2.77$ and $n = 0$ $E_0 = \hbar\Omega_0 = 1.0$ meV, $V_0 = -10$ meV, $a_w = 33.7$ nm, and $\beta a_w^2 = 3.41$.

at $X = 3.67$. At the broader peak at $X = 4.3$ the same also happens for the odd modes $n = 2$ and $n = 4$.

As expected, for higher energy the conductance of the broad wire becomes similar for the small and the larger dots except for the Fano resonances that represent quasi-bound states present in the energy continuum that depend on the shape of the pertinent dots.

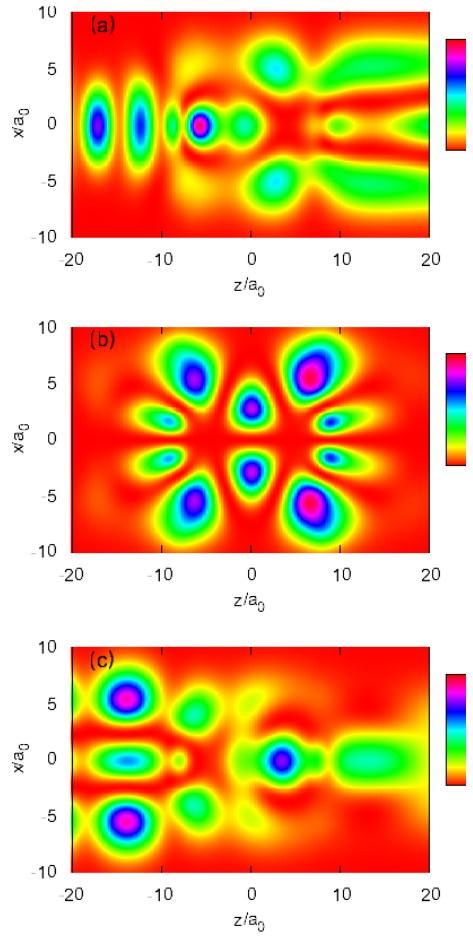

Fig. 9. (Color online) The probability density of the scattering state $\psi_E(x, y)$ in the broad quantum wire in the presence of two large embedded dots centered at $z = \pm 8a_0$. The incident energy and modes correspond to: (a) $X = 3.67$ and $n = 0$, (b) $X = 3.67$ and $n = 1$, and (c) $X = 3.67$ and $n = 2$ $E_0 = \hbar\Omega_0 = 1.0$ meV, $V_0 = -10$ meV, $a_w = 33.7$ nm, and $\beta a_w^2 = 3.41$.

4 Summary

We have explored the transport through a quantum wire with two embedded quantum dots that are not broader than the wire. We find in the transport an interplay between intra- and inter-dot scattering processes. We observe resonant transport through quasi bound states in the dots and also through resonances or quasi bound states between the dots. The interdot resonance states would have been very hard to identify without the help of the electron probability density.

By tuning the energy we can identify situations where the electron waves seem to be reflected by only one or the other embedded dot in the wire. Here is though important to have in mind that we are indeed observing a wave phenomenon that can not be arbitrarily localized in space.

In particular, we find for the larger dots in a broad wire drastic expamles of nonadiabatic transport [14]. Bryant explores the transport through a hard-wall quantum wire with a quantum dot defined by a tapered center and

separated from the wire region by two rectangular barriers [14]. He finds the mode-mixing effects to be more important when the transmission occurs by resonant tunneling and when the tapering is not quite smooth. Here we observe strong mode-mixing in ballistic transport when the energy subbands of the wire are closely spaced on the scale of the depth of the quantum dots and the size of the dots results in large matrix elements between the various transverse modes. Here is important that the symmetry of the centered dots establishes selection rules for the matrix elements that are thus of very variable magnitude. Also, even though one quantum dot of Gaussian shape can be considered smooth, then it is more difficult to measure the smoothness of the system of two smooth dots very well separated.

The methods employed to calculate the conductance have been applied to wires with parabolic (here) and hard wall confinement [23] in the transverse direction and are applicable to general scattering potentials as long as care is taken in selecting a sufficient number of input modes. This method has also been extended to a wire system in a homogeneous external magnetic field [25].

The research was partly financed by the Research and Instruments Funds of the Icelandic State, and the Research Fund of the University of Iceland. C.S.T. acknowledges computational facilities supported by the National Center for High-performance Computing in Taiwan.

References

1. R.H. Blick, R.J. Haug, J. Weis, D. Pfannkuche, K.V. Klitzing, K. Eberl, Phys. Rev. B **53**, 7899 (1996)
2. R.H. Blick, D. Pfannkuche, R.J. Haug, K. Klitzing, K. Eberl, Phys. Rev. Lett. **80**, 4032 (1998)
3. H. Jeong, A.M. Chang, M.R. Melloch, Science **293**, 2221 (2001)
4. A.W. Holleitner, R.H. Blick, A.K. Hüttel, K. Eberl, J.P. Kotthaus, Science **297**, 70 (2002)
5. M. Rontani, S. Amaha, K. Muraki, F. Manghi, E. Molinari, S. Tarucha, D.G. Austing, Phys. Rev. B **69**, 085327 (2004)
6. N.J. Craig, J.M. Taylor, E.A. Lester, C.M. Marcus, M.P. Hanson, A.C. Gossard, Science **304**, 565 (2004)
7. G. Klimeck, G. Chen, S. Datta, Phys. Rev. B **50**, 2316 (1994)
8. C. Niu, L. jun Liu, T. han Lin, Phys. Rev. B **51**, 5130 (1994)
9. C.A. Stafford, S.D. Sarma, Phys. Rev. Lett. **72**, 3590 (1994)
10. A. Aharony, O. Entin-Wohlmann, Y. Imry, Y. Levinson, Phys. Rev. B **62**, 13561 (2000)
11. P.A. Orellana, G.A. Lara, E.V. Anda, Phys. Rev. B **65**, 155317 (2002)
12. M.L.L. de Guevara, F. Claro, P.A. Orellana, Phys. Rev. B **67**, 195335 (2004)
13. V. Moldoveanu, A. Aldea, B. Tanatar, Phys. Rev. B **70**, 085303 (2004)
14. G.W. Bryant, Phys. Rev. B **44**, 12837 (1991)
15. C.S. Kim, A.M. Satanin, Y.S. Joe, R.M. Cosby, Phys. Rev. B **60**, 10962 (1999)
16. S.A. Gurvitz, Y.B. Levinson, Phys. Rev. B **47**, 10578 (1993)
17. J.U. Nöckel, A.D. Stone, Phys. Rev. B **50**, 17415 (1994)
18. R.L. Schult, D.G. Ravenhall, H.W. Wyld, Phys. Rev. B **39**, 5476 (1989)
19. C.C. Wan, T.D. Jesus, H. Guo, Phys. Rev. B **57**, 11907 (1998)
20. C.S. Tang, C.S. Chu, Physica B **292**, 127 (2000)
21. H. Xu, Phys. Rev. B **50**, 8469 (1994)
22. A.-P. Jauho, N.S. Wingreen, Y. Meir, Phys. Rev. B **50**, 5528 (1994)
23. J.H. Bardarson, I. Magnusdottir, G. Gudmundsdottir, C.-S. Tang, A. Manolescu, V. Gudmundsson, Phys. Rev. B **70**, 245308 (2004)
24. V. Vargiamidis, O. Valassiades, J. Appl. Phys. **92**, 302 (2002)
25. V. Gudmundsson, Y.-Y. Lin, C.-S. Tang, V. Moldoveanu, J.H. Bardarson, A. Manolescu, Phys. Rev. B **71**, 235302 (2005)
26. V. Vargiamidis, H.M. Polatoglou, Phys. Rev. B **71**, 075301 (2005)
27. J. Taylor, H. Guo, J. Wang, Phys. Rev. B **63**, 245407 (2001)
28. M.D. Ventra, S.T. Pantelides, N.D. Lang, Phys. Rev. Lett. **84**, 979 (2000)
29. J. Wang, H. Guo, Appl. Phys. Lett. **60**, 654 (1992)
30. S. Tarucha, D.G. Austing, T. Honda, R.J. van der Hage, L.P. Kouwenhoven, Phys. Rev. Lett. **77**, 3613 (1996)
31. L.P. Kouwenhoven, C.M. Marcus, P.L. McEuen, S. Tarucha, R.M. Westervelt, N.S. Wingreen, in *Mesoscopic Electron Transport*, edited by L.L. Sohn, L.P. Kouwenhoven, G. Schön, NATO Advanced Study Institute (Kluwer, Dordrecht, 1997), Vol. 345 of *Series E*
32. P.F. Bagwell, Phys. Rev. B **41**, 10354 (1990)
33. G. Cattapan, E. Maglione, Am. J. Phys. **71**, 903 (2003)
34. M. Buttiker, Y. Imry, R. Landauer, S. Pinhas, Phys. Rev. B **31**, 6207 (1985)
35. D.S. Fisher, P.A. Lee, Phys. Rev. B **23**, 6851 (1981)